Electronic structure and anomalous Hall effect in the ferromagnetic 3d-5d superlattice SrMnO_{3}/SrIrO_{3}

Sayantika Bhowal and S. Satpathy

Phys. Rev. B **99**, 245145 — Published 25 June 2019

DOI: 10.1103/PhysRevB.99.245145

Electronic Structure and the Anomalous Hall Effect in the Ferromagnetic $3d$-$5d$ superlattice: $SrMnO_3/SrIrO_3$

Sayantika Bhowal[1,*] and S. Satpathy[1]

[1]*Department of Physics & Astronomy, University of Missouri, Columbia, MO 65211, USA*

(Dated: June 10, 2019)

The electronic structure and the anomalous Hall effect (AHE) at the recently grown $3d$-$5d$ superlattice structure $(SrMnO_3)_1/\ (SrIrO_3)_1$ are investigated theoretically using model and density-functional calculations. The observed ferromagnetism for the SMO layer, which becomes electron doped because of the charge transfer across the interface, is explained to be due to the Anderson-Hasegawa double exchange, while the SIO side becomes ferromagnetic due to the proximity effect and the Nagaoka physics of a hole-doped system. The broken time-reversal symmetry and the strong spin-orbit coupling in SIO provide the two essential ingredients for the AHE, which we describe within a square lattice model of d-orbitals relevant for the present structure. The model correctly predicts the order of magnitude of the anomalous Hall conductivity (AHC), which is computed using the Kubo formula. The density-functional results for the AHC are in good agreement with the experiments.

I. INTRODUCTION

In the ordinary Hall effect, the Lorentz force acts on the electrons in a current carrying conductor in the presence of an external magnetic field, resulting in a transverse voltage[1]. In a broken time-reversal system, such as a ferromagnet, the Hall resistivity (R_H) has an anomalous contribution (R_s), which is usually an order of magnitude larger than the ordinary one (R_0)[2–4], so that $R_H = R_0B + R_sB_M$, where B is the applied magnetic field and B_M is the internal magnetic field of the ferromagnetic sample.

Although already noted by Hall himself in his original paper, an explanation of the anomalous Hall effect (AHE) had to wait for the discovery of the electron spin. Some seventy years after Hall's original work, the effect was finally explained in a seminal paper by Karplus and Luttinger[4], who attributed the effect to the spin-orbit coupling (SOC) forces, that induce a left-right asymmetry in the motion of the opposite spins. This so-called "intrisic" AHE was elegantly reformulated in terms of the Berry curvature of the Bloch states[5–7]. The Berry phase correction to the electron group velocity provides a successful explanation of the AHE in the solids, which can be computed using the density functional theory[8–10].

Recently, there have been several studies[11–16] of the interfaces between the $3d$ and $5d$ transition metal oxides (TMOs), both for fundamental new physics in the large SOC systems and for potential spintronics device applications[11]. In particular, the AHE has been measured for the (001) interface between $SrMnO_3$ (SMO) and $SrIrO_3$ (SIO), which has been experimentally grown and studied, where neither of the parent materials is ferromagnetic[11]. The observed AHC has been attributed to the ferromagnetism that emerges due to a charge transfer across the interface, which leads to a strong coupling between the two compounds. The presence of the AHE becomes evident from the non-linear hysteresis loop in the temperature dependent Hall resistance of $(SMO)_1/(SIO)_1$, a typical signature of the AHE. Interestingly, the ferromagnetism at the interface of the (001) superlattice structure $(SMO)_n/(SIO)_n$ grown on the $SrTiO_3$ substrate gradually decreases for $n > 1$ and eventually disappears at $n = 4$. As a consequence, the AHC is found to be maximum for the $(SMO)_1/(SIO)_1$ superlattice and decreases for large-period samples[11]. Additionally, in spite of recent theoretical work[16], the origin of the charge transfer as well as the mechanism of the ferromagnetism at the interface remain ill-understood.

In this paper, we study the anomalous Hall effect in the $(SMO)_1/(SIO)_1$ superlattice from density-functional calculations. The electronic structure is studied and the ferromagnetism at the interface is explained in terms of the charge transfer across the interface. On the SMO side, the ferromagnetism is described by the Anderson-Hasegawa double exchange physics, while on the SIO side, it is attributed to a combination of the proximity effect (exchange interaction across the interface) and the Nagaoka physics of a hole-doped half-filled Mott-Hubbard insulator. The magnetization computed from the density-functional theory (DFT) is found to be parallel to the c-axis (out of the plane) in line with the experimental observation. A model Hamiltonian for the d-orbitals on a square lattice in presence of the SOC and exchange splitting is employed to gain insight into the non-zero Berry curvature and the AHC in the system. The results of our model calculations are validated from the DFT calculations, and the computed AHC, a manifestation of the geometric property of the band structure, is found to be in good agreement with the experimental results.

The remaining parts of the paper are organized as follows. A description of the $(SMO)_1/(SIO)_1$ superlattice structure and the computational techniques is given in section II. This is followed by the DFT results for the electronic and magnetic structure in Sec. III, which also includes a description of the suggested mechanism for the magnetism. In Sec. IV, we illustrate the observed

AHC at the superlattice structure using a model Hamiltonian for d-orbitals on a square lattice, appropriate for the present system. This is followed by the DFT results for the AHC of the superlattice. Finally a summary of our work is presented in Sec. V.

II. STRUCTURAL AND COMPUTATIONAL DETAILS

The unit cell of the $(SMO)_1/(SIO)_1$ superlattice (Fig. 1) contains two formula units of SMO and SIO unless stated otherwise. The bulk SMO crystallizes in the cubic perovskite structure with ideal MnO_6 octahedra. On the other hand, SIO crystallizes in the orthorhombic perovskite structure, where the IrO_6 octahedron undergoes an orthorhombic distortion. The superlattice has a tetragonal structure as shown in Fig. 1 (a) with the in-plane lattice parameters ($a = b$) matched with the experimental lattice constant of the substrate $SrTiO_3$ (3.905 $\times\sqrt{2}$ Å) and the out-of-plane lattice parameters are fixed to the corresponding lattice constants of the bulk structures *i.e*, 3.80 Å for SMO[17] and 3.94 Å for SIO[18,19]. As shown in Fig. 1 (b), both Mn and Ir atoms are arranged on a square lattice.

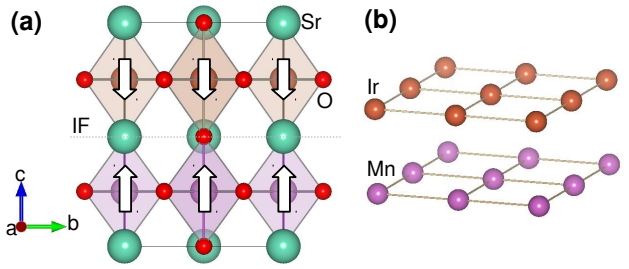

FIG. 1: The $(SMO)_1/(SIO)_1$ superlattice structure, showing the unit cell (a) and the square lattice formed by Ir and Mn atoms on either side of the interface (IF) (b). The arrows indicate the spins of the Mn and Ir atoms as obtained from the DFT calculations.

In order to study the magnetic properties of the superlattice, DFT calculations were performed using the plane-wave based projector augmented wave (PAW)[20,21] method as implemented in the Vienna *ab initio* simulation package (VASP)[22] within the generalized gradient approximation (GGA)[23] including Hubbard U[24] and SOC. The kinetic energy cut-off of the plane wave basis was chosen to be 550 eV. Following earlier authors[16], calculations were performed using U = 2 eV for Ir and U = 3 eV for Mn, unless stated otherwise.

The AHC of the superlattice structure was calculated using QUANTUM ESPRESSO and the Wannier interpolation approach[25,26]. Self-consistency with magnetization along the (001) direction was achieved using fully relativistic norm-conserving pseudopotentials and the PBE generalized-gradient approximation[23] for the exchange-correlation functional. Following a self-consistent calculation with total energy convergence of 10^{-8} Ry, the maximally-localized Wannier functions[27] were computed using the Wannier90 code[28] from the *ab-initio* ground state wave function obtained using a non-self-consistent calculation on a regular 8×8×4 k-mesh. Finally, the AHC was calculated by computing the Berry curvature using the Wannier interpolation approach[26]. The Brillouin zone (BZ) integration of the Berry curvature was carried out using a mesh up to 300×300×150 k-points with an adaptively refined mesh of 7×7×7 for the case when the absolute value of the sum of the Berry curvature over the occupied bands at a k point became larger than 100 Å^2. Calculation with finer mesh confirms the convergence of the calculated AHC. Some additional details of the calculations are presented in the Supplemental Materials[29].

III. ELECTRONIC STRUCTURE AND THE MAGNETIC PROPERTIES OF THE $(SMO)_1/(SIO)_1$ SUPERLATTICE

A. Density functional results

In this subsection, we discuss the electronic structure and magnetic properties of the $(SMO)_1/(SIO)_1$ superlattice structure obtained from the DFT calculations.

Bulk materials – The electronic structures of the two constituent bulk materials are well understood. In bulk SMO, Mn atoms are in the 4+ charge state, with three electrons occupying the t_{2g} orbitals, separated from the unoccupied e_g states by a large crystal field splitting. The Mn spins interact via a nearest-neighbor (NN) super exchange, stabilizing a G-type anti-ferromagnetic (AFM) insulating state with magnetic moment 2.77 μ_B/Mn, in good agreement with the experimental result of 2.6 ± 0.2 μ_B[17]. The strength of the NN AFM exchange J can be estimated by mapping the energy difference between the ferromagnetic (FM) and AFM configurations to the Heisenberg spin model. The calculated AFM interaction $J \approx 9$ meV is similar to that of the analogous compound $CaMnO_3$ ($J \approx 13$ meV). In an earlier work, we have discussed the mechanism of the super exchange interaction in the entire class of the colossal magnetoresistive manganites, of which SMO is a member[31].

The electronic structure of the bulk SIO, on the other hand, is to a large extent governed by the strong SOC of the 5d transition metal (TM) atom Ir. In bulk SIO, the Ir atoms are also in the 4+ charge state with t_{2g}^5 electronic configuration. Owing to the strong SOC, these t_{2g} states split into a completely filled $J_{\text{eff}} = 3/2$ quartet and a half-filled $J_{\text{eff}} = 1/2$ doublet. Our DFT calculations using U = 2 eV for the bulk SIO shows a canted AFM insulating ground state (see the Supplemental Materials[29]) with the spin and orbital moments of 0.34 μ_B/Ir and 0.22 μ_B/Ir

respectively. The canted AFM configuration for the bulk SIO is consistent with the magnetic insulating state reported in earlier calculations[32]. The small energy difference among the various magnetic configurations [see Table II of the Supplemental Materials[29]] is consistent with the paramagnetic behavior, observed experimentally[18]. The insulating ground state obtained from the DFT calculations for the bulk is also consistent with the reported transport property[18], which shows an insulator to metal transition at $T_{MI} \sim 44$ K with the low temperature structure being insulating. Indeed, experiments[33] have found that the paramagnetic metallic state of SIO is in close proximity to an AFM insulating state.

Superlattice – For the $(SMO)_1/(SIO)_1$ superlattice, the magnetic structure is drastically different from the bulk, both from experiments and theory. DFT calculations within the GGA+SOC+U functional show that both the SMO and SIO sides become FM, while the Ir and Mn spins are aligned antiferromagnetically with each other, as sketched in Fig. 1 (a). Calculations with U = 2 eV for Ir and U = 3 eV for Mn show that the spin moments at the Mn and Ir sites are altered, enhanced in one case and reduced in the other as compared to the corresponding bulk values (3.23 μ_B/Mn vs. 2.77 μ_B/Mn for the bulk and 0.21 μ_B/Ir vs. 0.34 μ_B/Ir for the bulk). Because the Ir and Mn moments are not the same in magnitude, a net FM moment emerges at the interface in agreement with the experiments[11]. As expected, the orbital moment at the Ir site is substantial (0.16 μ_B) due to the spin-orbital entanglement, while it is small for the Mn site (0.03 μ_B). Furthermore, comparison of the total energies (see Table I) for the constrained spin directions, viz., along $\hat{x}$, $\hat{y}$, or $\hat{z}$, indicates that the spins prefer to be aligned along the $\hat{z}$ direction consistent with the experimentally observed easy axis[11]. Test calculations with different values of U (U = 0.8. 1, 1.5 eV) at the Ir site showed that although the magnetic moment at the Ir site increases with U (0.11 μ_B/Ir at U = 0.8 eV to 0.21 μ_B/Ir at U = 2 eV), the ferromagnetic nature at the interface remains unchanged.

TABLE I: Total energies of the superlattice structure shown in Fig. 1 (a), with the spins constrained along $\hat{x}$, $\hat{y}$, or $\hat{z}$. Energy for the last case is set to zero.

Spin direction	ΔE (meV/fu)
$\hat{x}$	6
$\hat{y}$	6
$\hat{z}$	0

In the $(SMO)_1/(SIO)_1$ superlattice, there is leakage of electrons from the SIO side to the SMO side. The layer-projected densities of states (DOS) for the ground-state magnetic structure, shown in Fig. 2, indicate that the Ir-$J_{\rm eff}$ = 1/2 (half filled in the bulk SIO) and the Mn-$e_g^{\uparrow}$ (empty in the bulk SMO) states occur in the same energy range. This leads to the electron transfer across the interface from the Ir-$J_{\rm eff}$ = 1/2 state to the Mn-$e_g^{\uparrow}$ states, as illustrated in Fig. 2 (c). Integration of the total DOS up to the Fermi energy (E_F) on each side of the interface shows that there is approximately 0.08 electron transfer from the Ir atom to the Mn atom. Since, the charges are projected within the atomic spheres, they are renormalized appropriately. The computed amount of charge transfer is also consistent with the area of the BZ occupied by the Mn like states in the band structure for the interface, as indicated from Fig. 6 (a), shown in Section IV. Experimentally, such a charge transfer has indeed been observed; however, the magnitude is much larger, viz., about 0.5 electron, which may be attributed to the ambiguity of partitioning charges in a solid. A detail understanding of this discrepancy would require further work. The charge transfer at the interface plays an important role in determining the magnetic structure, which we discuss below.

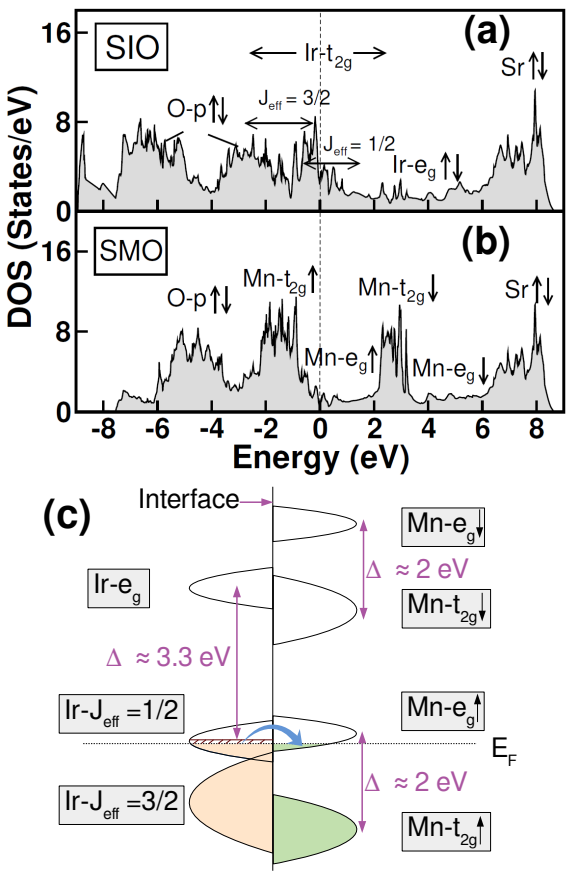

FIG. 2: Layer projected DOS for the $(SMO)_1/(SIO)_1$ superlattice (a, b). Fig. (c) illustrates the charge transfer across the interface from the half filled Ir-$J_{\rm eff}$ = 1/2 state in the bulk to the Mn-$e_g \uparrow$ state, which was unoccupied in the bulk SMO, resulting in an electron-doped SMO layer and a hole-doped SIO layer [see also the band structure in Fig. 6 (a)]. Fig. (c) also indicates the crystal field splittings Δ.

B. Ferromagnetism of the SIO layer: Magnetic Proximity Effect and Nagaoka Physics

The ferromagnetism in the SIO layer is a combination of magnetic proximity effect and hole doping. In presence of the neighboring ferromagnetic SMO layer (the ferromagnetism in the SMO layer is discussed below in section III C), the magnetic proximity effect arises due to the AFM coupling of the Ir atoms with the Mn atoms. DFT calculations show a strong (antiferromagnetic) exchange interaction between the Ir and Mn atoms across the interface, which drives the SIO layer ferromagnetic in order to align it with the ferromagnetic moments of the SMO layer. In addition, the charge transfer from the SIO side to the SMO side makes the SIO side hole doped, which favors a ferromagnetic alignment of the magnetic moments in the SIO side due to the Nagaoka physics. According to the Nagaoka theorem[34], in the strong coupling limit ($U/W \to \infty$) the AFM state of the half-filled Hubbard model can be destroyed by a single hole. However, for a finite U (typically ~ 2 eV for iridates), a critical hole concentration is needed for the system to be FM. Explicit mean-field calculations of the hole-doped Hubbard model show a FM ground state above a critical hole concentration (typically a few percent), the exact value of which depends on the U/W ratio[35]. In fact, a short-range ferromagnetism is observed experimentally in the hole doped bulk SIO[36], as suggested by the Nagaoka Theorem. Thus, the combination of the magnetic proximity effect and the Nagaoka physics provide a qualitative explanation of the observed ferromagnetism on the SIO side.

C. Ferromagnetism of the SMO layer: Andersen-Hasegawa Double exchange

The ferromagnetism of the electron-doped SMO layer as seen from the DFT calculations, discussed above, can be understood in terms of the Anderson-Hasegawa double exchange (DEX)[37,38], well known from the manganites physics. The essential physics of the DFT results for the ferromagnetism, therefore, can be captured by the tight-binding Hamiltonian discussed in this Section.

As a result of the transfer of electrons from the SIO side to the SMO side, the SMO layer becomes electron doped. The leaked electrons occupy the empty e_g states. The kinetic energy gain of these itinerant e_g electrons compete against the AFM superexchange of the core t_{2g} spins and depending on the doped electron concentration (x) a FM state can be stabilized at the electron doped SMO side. The hopping of the e_g electrons is a dynamic process making the Mn atom go between the two oxidation states Mn^{3+} and Mn^{4+}, with the average electron occupation of $t_{2g}^3 e_g^x$ on each Mn atom.

To describe this double exchange physics, we consider the tight-binding (TB) Hamiltonian for Mn atoms on a square lattice, appropriate for the SMO layer,

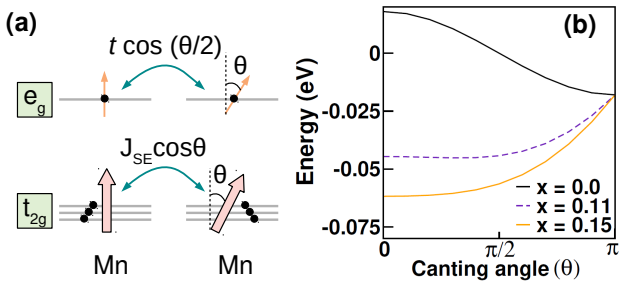

FIG. 3: The DEX mechanism for ferromagnetism for the electron doped SMO layer. (a) Schematic diagram indicating the Anderson-Hasegawa $t\cos\theta/2$ hopping and the super exchange $J_{\rm SE}$ between the core spins. (b) Total energy of the canted state as a function of the canting angle θ obtained from the model TB Hamiltonian (1). For small doping x, the AFM ground state turns into a canted ground state and eventually into a FM state for $x \gtrsim 0.11$ as seen from the figure.

$$\mathcal{H} = -t\cos(\theta/2)\sum_{\langle ij\rangle}(c^\dagger_{i\uparrow}c_{j\uparrow} + H.c.) + \sum_{\langle ij\rangle} J_{\rm SE}\ \hat{S}_i\cdot\hat{S}_j, \quad (1)$$

where $t\cos(\theta/2)$ is the Anderson-Hasegawa DEX hopping term for the itinerant e_g electrons, with the Hund's coupling $J_H \to \infty$, $J_{\rm SE}$ is the super exchange between the t_{2g}^3 core spins, and θ is the canting angle. We have considered a two-sublattice structure where within the sublattice the spins are FM, while the spins on the two different sublattices are canted with respect to each other with canting angle θ (Fig. 3 (a)). In manganites, J_H is typically ≈ 1 eV. For t_{2g}^3 core spin, therefore, the typical energy scale is ≈ 3 eV, justifying our infinite J_H approximation in obtaining the qualitative results for the present problem[39,40].

The total energy for the canted state is shown in Fig. 3 for several doping levels as obtained from the TB model, Eq. (1). The results indicate that the ground-state changes from AFM for the undoped case, to a canted state for small doping x, and eventually to a FM state for $x \geq x_c$, with a critical concentration $x_c \sim 0.11$. This result is easily understood with the reasonable approximation, originally due to de Gennes[38], that all doped electrons occupy the band bottom E_b, so that $E = E_b x + 2J_{\rm SE}\cos\theta$. With $E_b = -4|t|\cos(\theta/2)$ for the square lattice, minimization of the total energy immediately yields the result for the canting angle $\theta = 2\cos^{-1}\left(\frac{|t|x}{2J_{\rm SE}}\right)$ for the ground state. A FM state is indicated when the argument exceeds one, with the result that $x_c = 2J_{\rm SE}/|t| \approx 0.11$, for $J_{\rm SE} = 9$ meV and $|t| = 0.17$ eV, which we have estimated from the band calculations for bulk SMO. This critical value x_c obtained from the de Gennes approximation is quite close to the value obtained from the full TB calculation shown in Fig. 3. We found a charge transfer of about 8% across the in-

terface from our DFT calculations, which although not more than the critical value obtained from this simplified model, is quite close to it, suggesting the DEX mechanism to be responsible for the ferromagnetic ground state on the SMO side. We also note that in the bulk SMO, experimentally, only about 5% dopant concentration x is needed to turn the doped SMO ferromagnetic from the original AFM ground state for the undoped case.

The theory of ferromagnetism in the $(SMO)_1(SIO)_1$ superlattice, as discussed above, can be directly extended to describe the magnetism in the large period superlattices $(SMO)_n(SIO)_n$ with $n \geq 2$. For the large period superlattices, the electrons leak into the SMO layers away from the interface in addition to the first interfacial SMO layer, leading to a reduced electron doping concentration in the first SMO layer. Such a reduced doping may not exceed the critical doping concentration for ferromagnetism, resulting in a canted anti-ferromagnetic structure due to DEX. This results in a smaller but non-zero net ferromagnetic moment in the $(SMO)_n(SIO)_n$ superlattices. Similar results hold for the SIO side due to the reduced hole concentration. Indeed, experiments[11] show a gradual reduction in the ferromagnetic moment from $n = 1$ to 3 that disappears completely for $n \geq 4$.

IV. ANOMALOUS HALL CONDUCTIVITY

In order to gain insight into the AHE of the $(SMO)_1/(SIO)_1$ superlattice, we first study the effect of the various physical parameters on the anomalous Hall conductivity using an appropriate tight-binding Hamiltonian, before we present the density-functional results.

The AHC ($\sigma_{xy}^{\rm AHC}$) can be calculated from the momentum sum of the Berry curvatures over the occupied electron states in the BZ[41],

$$\sigma_{xy}^{\rm AHC} = -\frac{e^2}{\hbar}\frac{1}{N_k\Omega_c}\sum_{\mathbf{k}}\Omega^z(\mathbf{k}), \qquad (2)$$

where $\Omega^z(\mathbf{k}) = \sum_n f(\varepsilon_{n\mathbf{k}})\Omega_n^z(\mathbf{k})$. Ω_c, N_k and $f(\varepsilon_{n\mathbf{k}})$ are respectively the cell volume, the number of k-points used for sampling the BZ, and the Fermi-Dirac distribution function. The Berry curvature $\Omega_n^z(\mathbf{k})$ of the $n^{\rm th}$ band is a geometric property of the band structure and can be calculated using the Kubo-formula[42]

$$\Omega_n^z(\mathbf{k}) = -2\hbar^2\sum_{n'\neq n}\frac{{\rm Im}\langle\psi_{n\mathbf{k}}|v_x|\psi_{n'\mathbf{k}}\rangle\langle\psi_{n'\mathbf{k}}|v_y|\psi_{n\mathbf{k}}\rangle}{(\varepsilon_{n'}-\varepsilon_n)^2}, \quad (3)$$

where the velocity operator $v_\eta = \frac{1}{\hbar}\frac{\partial H}{\partial k_\eta}, \eta = x$ or y, and ε_n and $\psi_{n\mathbf{k}}$ are the band energies and the wave functions.

We consider a TB model for d orbitals on a square lattice with broken time-reversal (TR) symmetry (ferromagnetism) and in the presence of SOC, which reads

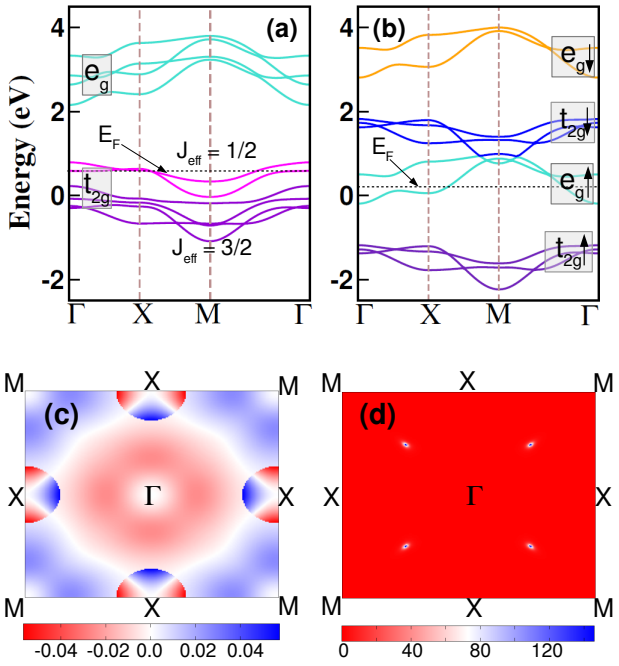

FIG. 4: Band structure and the corresponding Berry curvature $\Omega_n^z(\mathbf{k})$ obtained from the tight-binding model Eq. 4 for SIO (*left*) and SMO (*right*). The Fermi energy E_F corresponds to the dopant concentration $x \approx 0.1$ as appropriate for the $(SIO)_1/(SMO)_1$ interface. For the Berry curvature $n = 5$ for SIO and 4 for SMO, which are the occupied bands closest to E_F.

$$\begin{aligned} H = \;& H_{kin} + H_{ex} + H_{soc} \\ = \;& \sum_{i\mu\sigma,j\nu\sigma} t_{ij}^{\mu\nu} c_{i\mu\sigma}^\dagger c_{j\nu\sigma} - J_{ex}\sum_{i\mu}\sum_{\sigma,\sigma'} c_{i\mu\sigma}^\dagger \sigma_{\sigma\sigma'}^z c_{i\mu\sigma'} \\ & + \frac{\lambda}{2}\sum_{i\eta}\sum_{\mu\sigma,\nu\sigma'} c_{i\mu\sigma}^\dagger L_{\mu\nu}^\eta \sigma_{\sigma\sigma'}^\eta c_{i\nu\sigma'}. \end{aligned} \qquad (4)$$

Here, $c_{i\mu\sigma}^\dagger$ creates an electron at the i-th site, with $\mu\sigma$ being the orbital and spin indices, $t_{ij}^{\mu\nu}$ is the TB hopping integral, which also includes the on-site energies (in particular, the t_{2g}-e_g splitting Δ), J_{ex} is the spin splitting, and λ is the SOC constant that couples the orbital ($\vec{L}$) and spin moments ($\vec{S} = \frac{1}{2}\vec{\sigma}$). The exchange splitting, the second term in the Hamiltonian, is consistent with the alignment of the magnetic moments along $\hat{z}$ as obtained from the DFT results.

The typical magnitudes of the hopping parameters in Hamiltonian (4) correspond to $V_\sigma = -0.2$ eV (1NN), -0.1 eV (2NN), and $V_\sigma/V_\pi = -1.85$ using the Harrison's table[43]. Guided by the DFT results, two different sets of parameters (Δ, J_{ex} and λ) are chosen for the description of the 5d (Ir) and 3d TM (Mn) atoms, viz., $\Delta = 3$ eV, $J_{ex} = -0.5$ eV, and $\lambda = 0.4$ eV for SIO, and $\Delta = 2$ eV, $J_{ex} = 3$ eV, and $\lambda = 0.1$ eV for SMO. These parameters

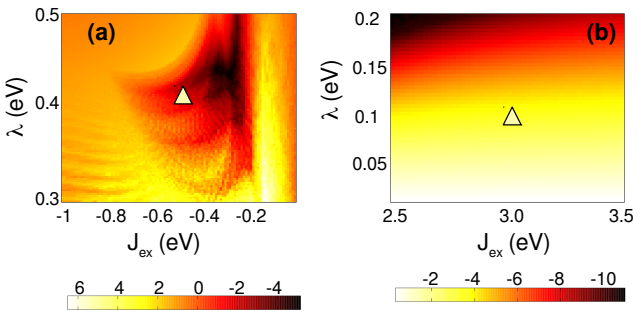

FIG. 5: Anomalous Hall conductivity (in units of $\Omega^{-1}\text{cm}^{-1}$) for the square-lattice model (4) as a function of λ and J_{ex} as appropriate for SIO (a) and SMO (b). We used the dopant concentration $x = 0.1$, electrons for SMO and holes for SIO, and the triangles indicate the parameters for the two materials.

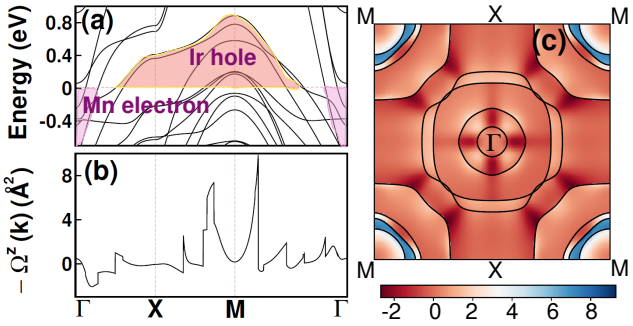

FIG. 6: DFT results for the $(SMO)_1/(SIO)_1$ superlattice: The band structure along high symmetry lines (a) and the Berry curvature sum $\Omega^z(\mathbf{k})$ (b). The Ir hole and Mn electron pockets are indicated by the shaded region in the band structure. The Berry curvature sum (in units of Å^2) in the $k_z = 0$ plane is shown in (c) with color coding, indicating that large contributions come from regions around the M point. The lines in (c) represent the locus of the momentum points where the various bands in (a) cross E_F.

reproduce the key features of the iridate and manganite band structures as shown in Fig. 4. Note that the opposite signs of J_{ex} for $5d$ and $3d$ TM atoms take care of the anti-parallel alignment of the Ir and Mn moments, as indicated in Fig. 1.

The broken TR symmetry of the Hamiltonian (4) ensures that $\Omega_n(\mathbf{k}) \neq -\Omega_n(-\mathbf{k})$, while the inversion symmetry enforces the condition $\Omega_n(\mathbf{k}) = \Omega_n(-\mathbf{k})$[44], which results in a non-zero Berry curvature. The magnetization along $\hat{z}$ ensures that $\Omega^z_n(\mathbf{k})$ is the only non-zero component of $\vec{\Omega}_n(\mathbf{k})$. The computed values using the Kubo formula (3), shown in Fig. 4 confirms the symmetry conditions for $\Omega^z_n(\mathbf{k})$ stated above. As seen from Fig. 4 (c) and (d), for both SIO and SMO, the Berry curvature is non-zero and is an even function of k_x and k_y as expected. Fig. 4 clearly shows that the contribution to the Berry curvature primarily comes from the band crossing regions, as anticipated from the Kubo formula (3).

It is important to note that an inter-orbital hopping is necessary to produce a non-zero AHE. As noted by Karplus and Luttinger, the intrinsic AHE, which is directly connected with the Berry curvature, is an inter-band process[4]. The inter-orbital hopping appears in the off-diagonal matrix element of the velocity operator, known as the anomalous velocity, and it is necessary for a non-zero Berry curvature[45]. For a t_{2g} only model this effect generally arises from the hopping between xz and yz orbitals[10]. In reality, such hoppings may arise even within the NN interactions due to hybridization of the TM-d orbitals with the ligand-p states. Within our square-lattice model (4), there is no inter-orbital hopping for the 1NN, and therefore the 2NN is necessary for the AHE, which has been included in our TB Hamiltonian.

The computed AHC for the TB model using the Berry curvature expressions Eqs. 2 and 3 are shown in Fig. 5 as a function of the SOC and exchange parameters λ and J_{ex}. As seen from the figure, the AHC is quite sensitive to these parameters, as they control the fine details of the band structure near the Fermi energy, which in turn affects the Berry curvature due to the energy denominator in the Kubo formula (3). The net AHC for our system is obtained from Fig. 5 by adding the individual contributions, indicated by the triangles in Fig. 5, for the two parts, SIO and SMO. The calculated value ($\approx 10\ \Omega^{-1}\text{cm}^{-1}$) correctly estimates the order of magnitude of the AHC, as obtained from the experiment as well as from our DFT calculations discussed below for the $(SMO)_1(SIO)_1$ superlattice structure. Note that in the present model, we have not explicitly included the coupling between the $3d$ and $5d$ TM atoms (Ir-Mn coupling), but it is taken care of indirectly by considering the magnetic structure, which results from the Ir-Mn coupling. In principle, a model including explicitly the Ir-Mn coupling can also be constructed, in which case, however, the simplicity of the essential physics would be lost. Nevertheless, the simple model presented in this section gives the qualitative understanding of the observed AHC at the interface.

Density-Functional Results – We computed the AHC from density-functional theory using the Wannier interpolation approach[26] as implemented in the Wannier90 code. The band structure of the superlattice near the Fermi energy along high symmetry lines is shown in Fig. 6 (a), where also the Mn electron and Ir hole pockets have been indicated. Note that in the figure, the Ir holes are missing electrons from the filled t^6_{2g} bands (both $J_{\text{eff}} = 3/2$ and $1/2$ bands are full). In bulk SIO, the doubly degenerate $J_{\text{eff}} = 1/2$ bands are only half full. The size of the electron and hole pockets indicated from Fig. 6 (a) is consistent with the charge transfer of $x \approx 0.08$ electrons from the half filled $J_{\text{eff}} = 1/2$ bands in bulk SIO to the empty Mn e_g bands in bulk SMO. Fig. 6 (b) shows the sum of the Berry curvatures over the occupied

states.

As seen from Fig. 6, the Berry curvature sum peaks around the M point, where the SOC splits the Ir-d bands in such a way that one of the bands is occupied, while the other is empty. The small energy difference between the bands leads to a large contribution to the Berry curvature due to the small energy denominator appearing in the Kubo formula (3). A pair of bands, split by SOC, do not contribute to the AHC if both of them are occupied. The Fermi surface and the Berry curvature in the $k_z = 0$ plane are shown in Fig. 6 (c). The large contribution to the total Berry curvature around the M point is also evident from this plot. The calculated value of the AHC obtained from the BZ sum of the Berry curvature Eq. 2 is 26 $\Omega^{-1}\text{cm}^{-1}$ in reasonable agreement with the experimental value of $\approx 18\ \Omega^{-1}\text{cm}^{-1}$[11]. Part of the difference could be due to the AHC due to extrinsic mechanisms not included in the band calculations.

V. SUMMARY

In summary, from model Hamiltonian as well as a density-functional calculation, we studied the interfacial magnetism and the AHC of the recently grown $3d$-$5d$ superlattice, viz., $(\text{SMO})_1/(\text{SIO})_1$. This superlattice is a notable example of the $3d$-$5d$ interface, where the strong coupling between the parent TMOs is achieved by the transfer of electrons across the interface.

Explicit model calculations were employed to gain insight into the DFT results and show that the charge transfer across the interface plays a crucial role in altering the magnetism at the interface. The doped electrons in SMO causes the magnetism to switch from AFM to FM via the double exchange mechanism, while the ferromagnetism in the hole doped SIO part can be explained by a combination of the magnetic proximity effect and the Nagaoka physics for hole-doped Hubbard model.

The net ferromagnetism at the interface together with a strong SOC of the Ir atoms leads to the AHE. Using a general model Hamiltonian for the TM-d orbitals on a square lattice, relevant for both SIO and SMO, we have shown that a non-zero Berry curvature exists for both sides. We noted that the 2NN inter-orbital hopping is necessary for the non-zero Berry curvature, and therefore for the AHE as well. The model Hamiltonian was studied as a function of the strengths of the exchange interaction and the SOC parameters J_{ex} and λ, which was used to interpret the DFT results. The calculated AHC of $\approx 26\ \Omega^{-1}\text{cm}^{-1}$ from DFT is in reasonable agreement with the experimental value[11]. Our work provides important insight into the AHE in the $3d$-$5d$ structures and suggests that the effect can be manipulated by changing the SOC strength and by controlling the amount of charge transfer, e. g., by a gate voltage or external strain. We hope that our work motivates further experimental work in this direction.

VI. ACKNOWLEDGMENTS

We thank the U.S. Department of Energy, Office of Basic Energy Sciences, Division of Materials Sciences and Engineering for financial support under Grant No. DEFG02-00ER45818.

* Electronic address: bhowals@missouri.edu

[1] E. H. Hall, On a New Action of the Magnet on Electric Currents, Am. J. Math. **2**, 287 (1879).
[2] E. H. Hall, On the new action of magnetism on a permanent electric current, Philos. Mag. **10**, 301 (1880).
[3] E. H. Hall, On the Rotational Coefficient in nickel and cobalt, Philos. Mag. **12**, 157 (1881).
[4] R. Karplus and J.M. Luttinger, Hall Effect in Ferromagnetics, Phys. Rev. **95**, 1154 (1954).
[5] Ming-Che Chang and Q. Niu, Berry Phase, Hyperorbits, and the Hofstadter Spectrum, Phys. Rev. Lett. **75**, 1348 (1995).
[6] Ming-Che Chang and Q. Niu, Berry phase, hyperorbits, and the Hofstadter spectrum: Semiclassical dynamics in magnetic Bloch bands, Phys. Rev. B **53**, 7010 (1996).
[7] G. Sundaram and Q. Niu, Wave-packet dynamics in slowly perturbed crystals: Gradient corrections and Berry-phase effects, Phys. Rev. B **59**, 14 915 (1999).
[8] T. Jungwirth, Q. Niu, and A. H. MacDonald, Anomalous Hall Effect in Ferromagnetic Semiconductors, Phys. Rev. Lett. **88**, 207208 (2002).
[9] Y. Yao, L. Kleinman, A. H. MacDonald, J. Sinova, T. Jungwirth, D.-S. Wang, E.-G. Wang, and Q. Niu, First Principles Calculation of Anomalous Hall Conductivity in Ferromagnetic bcc Fe, Phys. Rev. Lett. **92**, 037204 (2004).
[10] H. Kontani, T. Tanaka, and K. Yamada, Intrinsic anomalous Hall effect in ferromagnetic metals studied by the multi-d-orbital tight-binding model, Phys. Rev. B **75**, 184416 (2007).
[11] J. Nichols, X. Gao, S. Lee, T. L. Meyer, J. W. Freeland, V. Lauter, D. Yi, J. Liu, D. Haskel, J. R. Petrie1, E.-J. Guo, A. Herklotz, D. Lee, T. Z. Ward, G. Eres, M. R. Fitzsimmons, and H. N. Lee, Emerging magnetism and anomalous Hall effect in iridate-manganite heterostructures, Nat. Commun. **7**, 12721 (2016).
[12] J. Matsuno, K. Ihara, S. Yamamura, H. Wadati, K. Ishii, V. V. Shankar, H.-Y. Kee, and H. Takagi, Engineering a Spin-Orbital Magnetic Insulator by Tailoring Superlattices, Phys. Rev. Lett. **114**, 247209 (2015).
[13] W. Fan and S. Yunoki, Electronic and Magnetic Structure under Lattice Distortion in $SrIrO_3/SrTiO_3$ Superlattice: A First-Principles Study, J. Phys.: Conf. Ser. **592**, 012139 (2015).
[14] B. Pang, L. Zhang, Y. B. Chen, J. Zhou, S. Yao, S. Zhang, and Y. Chen, Spin-Glass-Like Behavior and Topological Hall Effect in $SrRuO_3/SrIrO_3$ Superlattices for Oxide Spintronics Applications, ACS Appl. Mater. Interfaces **9**, 3201-3207 (2017).

[15] J.-W. Kim, Y. Choi, S. H. Chun, D. Haskel, D. Yi, R. Ramesh, J. Liu, and P. J. Ryan, Controlling entangled spin-orbit coupling of 5d states with interfacial heterostructure engineering, Phys. Rev. B **97**, 094426 (2018).

[16] S. Okamoto, J. Nichols, C. Sohn, S. Y. Kim, T. W. Noh, and H. N. Lee, Charge Transfer in Iridate-Manganite Superlattices, Nano Lett. **17**, 2126-2130 (2017).

[17] T. Takeda and S. Ohara, Magnetic Structure of the Cubic perovskite Type $SrMnO_3$, J. Phys. Soc. Jpn. **37**, 275 (1974).

[18] J. G. Zhao, L. X. Yang, Y. Yu, F. Y. Li, R. C. Yu, Z. Fang, L. C. Chen, and C. Q. Jin, High-pressure synthesis of orthorhombic $SrIrO_3$ perovskite and its positive magnetoresistance, J. Appl. Phys. **103**, 103706 (2008).

[19] J. M. Longo, J. A. Kafalas, and R. J. Arnott, Structure and Properties of the High and Low Pressure Forms of $SrIrO_3$, J. Solid State Chem. **3** 174 (1971).

[20] P. E. Blochl, Projector augmented-wave method, Phys. Rev. B **50**, 17953 (1994).

[21] G. Kresse and D. Joubert, From ultrasoft pseudopotentials to the projector augmented-wave method, Phys. Rev. B **59**, 1758 (1999).

[22] G. Kresse and J. Furthmüller, Efficient iterative schemes for *ab initio* total-energy calculations using a plane-wave basis set, Phys. Rev. B **54**, 11169 (1996).

[23] J. P. Perdew, K. Burke, and M. Ernzerhof, Generalized Gradient Approximation Made Simple, Phys. Rev. Lett. **77**, 3865 (1996).

[24] V. I. Anisimov, J. Zaanen, and O. K. Andersen, Band theory and Mott insulators: Hubbard U instead of Stoner I, Phys. Rev. B **44**, 943 (1991).

[25] P. Giannozzi, S. Baroni, N. Bonini, M. Calandra, R. Car, C. Cavazzoni, D. Ceresoli, G. L. Chiarotti, M. Cococcioni, I. Dabo, QUANTUM ESPRESSO: a modular and open-source software project for quantum simulations of materials, J. Phys. Condens. Matter **21**, 395502 (2009).

[26] X.Wang, J. R. Yates, I. Souza, and D. Vanderbilt, Ab initio calculation of the anomalous Hall conductivity by Wannier interpolation, Phys. Rev. B **74**, 195118 (2006).

[27] N. Marzari and D. Vanderbilt, Maximally localized generalized Wannier functions for composite energy bands, Phys. Rev. B **56**, 12847 (1997).

[28] A. A. Mostofi, J. R. Yates, Y.-S. Lee, I. Souza, D. Vanderbilt, and N. Marzari, wannier90: A tool for obtaining maximally-localised Wannier functions, Comput. Phys. Commun. **178**, 685 (2008).

[29] Supplemental Materials describing the density functional results for magnetism in the bulk SIO and details of the AHC calculation for $(SIO)_1(SMO)_1$ superlattice, which include Ref. 30.

[30] J. M. Perez-Mato, S.V. Gallego, E.S. Tasci, L. Elcoro, G. de la Flor, and M.I. Aroyo, Symmetry-Based Computational Tools for Magnetic Crystallography, Annu. Rev. Mater. Res. **45**, 217 (2015).

[31] H. Meskine, H. König, and S. Satpathy, Orbital ordering and exchange interaction in the manganites, Phys. Rev. B **64**, 094433 (2001).

[32] M. A. Zeb, and H.-Y. Kee, Interplay between spin-orbit coupling and Hubbard interaction in $SrIrO_3$ and related *Pbnm* perovskite oxides, Phys. Rev. B **86**, 085149 (2012).

[33] H. Zheng, J. Terzic, F. Ye, X. G. Wan, D. Wang, J. Wang, X. Wang, P. Schlottmann, S. J. Yuan, and G. Cao, Simultaneous metal-insulator and antiferromagnetic transitions in orthorhombic perovskite iridate $Sr_{0.94}Ir_{0.78}O_{2.68}$ single crystals, Phys. Rev. B **93**, 235157 (2016).

[34] Y. Nagaoka,Ferromagnetism in a Narrow, Almost Half-Filled *s* Band, Phys. Rev. **147**, 392 (1966).

[35] J. M. Kurdestany and S. Satpathy, Mott metal-insulator transition in the doped Hubbard-Holstein model, Phys. Rev. B **96**, 085132 (2017).

[36] Qasim, I., Kennedy, B. J. & Avdeev, M. Stabilising the orthorhombic perovskite structure in SrIrO3 through chemical doping. Synthesis, structure and magnetic properties of $SrIr_{1-x}Mg_xO_3$ ($0.20 \leq x \leq 0.33$), J. Mater. Chem. A **1**, 13357 (2013).

[37] P. W. Anderson and H. Hasegawa, Considerations on Double Exchange, Phys. Rev. **100**, 675 (1955).

[38] P.-G. de Gennes, Effects of double exchange in magnetic crystals, Phys. Rev. **118**, 141 (1960).

[39] S. Satpathy, Z. S. Popović, and F. R. Vukalović, Electronic structure of the perovskite oxides La_{1-x} Ca_xMnO_3, Phys. Rev. Lett. **76**, 960 (1986).

[40] S. K. Mishra, S. Satpathy, F. Aryasetiawan, and O. Gunnarsson, Possible suppression of canted spin order in the double-exchange lanthanum manganites, Phys. Rev. B **55**, 2725 (1997).

[41] M.-C. Chang and Q. Niu, Berry Phase, Hyperorbits, and the Hofstadter Spectrum, Phys. Rev. Lett. **75**, 1348 (1995); Berry phase, hyperorbits, and the Hofstadter spectrum: Semiclassical dynamics in magnetic Bloch bands, Phys. Rev. B **53**, 7010 (1996).

[42] D. J. Thouless, M. Kohmoto, M. P. Nightingale, and M. den Nijs, Quantized Hall Conductance in a Two-Dimensional Periodic Potential, Phys. Rev. Lett. **49**, 405 (1982).

[43] W. A. Harrison, Electronic Structure and the Properties of Solids (Dover, New York, 1989).

[44] H. Chen, Q. Niu, and A. H. MacDonald, Anomalous Hall Effect Arising from Noncollinear Antiferromagnetism, Phys. Rev. Lett. **112**, 017205 (2014). Breaking of either inversion or TR symmetry leads to non-zero Berry curvature in the system.

[45] S. Bhowal and S. Satpathy, Electric Field Tuning of the Anomalous Hall Effect at oxide interfaces, arXiv:1812.08950v1 (2018). A pedagogical discussion of this point is given in the Supplementary Materials.